Genetic architecture of natural variation in visual senescence in *Drosophila*

Mary Anna Carbone[a,b,c], Akihiko Yamamoto[a,b,c], Wen Huang[a,b,c,d], Rachel A. Lyman[a,1], Tess Brune Meadors[a], Ryoan Yamamoto[a], Robert R. H. Anholt[a,b,c,d], and Trudy F. C. Mackay[a,b,c,d,2]

[a]Department of Biological Sciences, North Carolina State University, Raleigh, NC 27695; [b]W. M. Keck Center for Behavioral Biology, North Carolina State University, Raleigh, NC 27695; [c]Program in Genetics, North Carolina State University, Raleigh, NC 27695; and [d]Initiative in Biological Complexity, North Carolina State University, Raleigh, NC 27695

Contributed by Trudy F. C. Mackay, August 27, 2016 (sent for review May 17, 2016; reviewed by Jeff Leips and Johanna Schmitt)

Senescence, i.e., functional decline with age, is a major determinant of health span in a rapidly aging population, but the genetic basis of interindividual variation in senescence remains largely unknown. Visual decline and age-related eye disorders are common manifestations of senescence, but disentangling age-dependent visual decline in human populations is challenging due to inability to control genetic background and variation in histories of environmental exposures. We assessed the genetic basis of natural variation in visual senescence by measuring age-dependent decline in phototaxis using *Drosophila melanogaster* as a genetic model system. We quantified phototaxis at 1, 2, and 4 wk of age in the sequenced, inbred lines of the *Drosophila melanogaster* Genetic Reference Panel (DGRP) and found an average decline in phototaxis with age. We observed significant genetic variation for phototaxis at each age and significant genetic variation in senescence of phototaxis that is only partly correlated with phototaxis. Genome-wide association analyses in the DGRP and a DGRP-derived outbred, advanced intercross population identified candidate genes and genetic networks associated with eye and nervous system development and function, including seven genes with human orthologs previously associated with eye diseases. Ninety percent of candidate genes were functionally validated with targeted RNAi-mediated suppression of gene expression. Absence of candidate genes previously implicated with longevity indicates physiological systems may undergo senescence independent of organismal life span. Furthermore, we show that genes that shape early developmental processes also contribute to senescence, demonstrating that senescence is part of a genetic continuum that acts throughout the life span.

aging | behavioral genetics | DGRP GWA analysis | phototaxis | xQTL mapping

Senescence—the decline in organismal functions with age—is a major determinant of health span in an aging population. In humans, visual decline (presbyopia) is a common phenomenon that heralds the onset of senescence after the age of 40. Age-related eye diseases, including macular degeneration (1), cataracts (2), diabetic retinopathy (3), and glaucoma (4), are the leading causes of vision impairment and blindness in the United States and are prevalent among Americans 40 y and older (5). Several disease mechanisms have been proposed, including the unfolded protein response (6, 7), the Wnt signaling pathway (8, 9), oxidative stress pathways (10, 11), and apoptosis (12, 13). In addition, an association between sleep disorders and eye disorders has been recognized (14). However, the genetic basis of interindividual variation in senescence within the normal range of visual decline remains largely unknown. Disentangling the genetic and environmental factors affecting human complex traits and disease is challenging due to large sample sizes needed to identify DNA variants with small phenotypic effects and uncontrolled variation due to different histories of environmental exposures and lifestyles. Furthermore, insidious onset of diseases with a diversity of phenotypic manifestations renders consistent phenotypic quantification challenging. Model organisms allow precise control of the genetic background and environmental rearing conditions and can provide generally applicable insights into the genetic underpinnings of complex traits and human diseases based on the principle of evolutionary conservation of fundamental cellular pathways.

Drosophila melanogaster has emerged as a powerful genetic model system for the study of complex human disorders (15) including Alzheimer's disease (16), Parkinson's disease (17), Huntington's disease (18), ocular hypertension (6), retinal degeneration (7), longevity (19), sleep patterns (20), aggressive behaviors (21–24), and sensitivity to alcohol (25–30). Natural populations of *Drosophila* harbor substantial genetic variation for quantitative traits (31–34). The *D. melanogaster* genome has been sequenced (35) and extensively annotated (36), and many mutant lines and RNAi knockdown constructs are publicly available (37–39). Furthermore, flies exhibit an innate phototaxis response—the locomotor response toward a light stimulus—that can be quantified for large numbers of age-synchronized individuals of the same sex and genotype under controlled environmental conditions (40). Large-scale genetic screens for phototaxis have provided insights into the cellular mechanisms of phototransduction (41) and identified over 100 mutations that affect the development of the visual system, photoreceptor cell integrity, and phototransduction (42). Similar to human age-related visual senescence, phototaxis in *Drosophila* exhibits age-related progressive decline (43–45).

Here we sought to answer three questions about the genetic basis of natural variation in phototaxis as well as age-dependent

Significance

Functional decline with age—senescence—is a major determinant of health span in an aging population, but its genetic basis remains largely unknown. In humans, visual decline often heralds the onset of senescence. We used the fruit fly, *Drosophila melanogaster*, to explore the genetic basis of natural variation in phototaxis, the innate tendency to move toward light, and age-dependent decline in phototaxis as a proxy for visual senescence. We found the genetic basis for visual senescence is distinct from that which determines variation in life span. Furthermore, genes shaping early development of the nervous system, in particular the visual system, also contribute to senescence at later age, demonstrating that senescence is part of a genetic continuum throughout the life span.

Author contributions: M.A.C., R.R.H.A., and T.F.C.M. designed research; M.A.C., A.Y., W.H., R.A.L., T.B.M., and R.Y. performed research; M.A.C., W.H., and T.F.C.M. analyzed data; and M.A.C., W.H., R.R.H.A., and T.F.C.M. wrote the paper.

Reviewers: J.L., University of Maryland, Baltimore County; and J.S., University of California, Davis.

The authors declare no conflict of interest.

Freely available online through the PNAS open access option.

[1]Present address: Department of Biology, Washington University, St. Louis, MO 63130.

[2]To whom correspondence should be addressed. Email: trudy_mackay@ncsu.edu.

This article contains supporting information online at www.pnas.org/lookup/suppl/doi:10.1073/pnas.1613833113/-/DCSupplemental.

decline in phototaxis as a proxy for visual senescence, using the *Drosophila* model. First, do the same genes that affect phototaxis also affect senescence for phototaxis? Second, do the same genes that affect eye and nervous system development affect natural variation in phototaxis and senescence for phototaxis? Third, are the genetic underpinnings of *Drosophila* phototaxis and phototaxis senescence specific to flies or evolutionarily conserved?

We performed genome-wide association (GWA) analyses using the sequenced, inbred lines of the *D. melanogaster* Genetic Reference Panel (DGRP) (46) as well as a large outbred advanced intercross population (AIP) derived from a subset of DGRP lines, which provides increased statistical power and the ability to detect variants that segregate with low minor allele frequencies in the DGRP. We find, perhaps surprisingly, that the genetic basis of phototaxis senescence is partly independent from that for phototaxis. We show that genes associated with early eye and nervous system development contribute to standing variation in phototaxis and also to variation in phototaxis senescence later in life. Finally, many of the genes and cellular pathways associated with variation in age-dependent decline in phototaxis in *Drosophila* are evolutionarily conserved, and their orthologs may contribute to age-related visual decline in vertebrates, including humans.

Results

Natural Variation in Phototaxis and Senescence in Phototaxis. To assess the magnitude of naturally occurring variation in phototaxis per se as well as genetic variation in phototactic senescence, we measured phototaxis of adult males and females from 191 DGRP lines at 1, 2, and 4 wk posteclosion, with a total sample size of n = 141,032 flies (Dataset S1). Averaged over all lines, phototaxis significantly declined between 1- and 4-wk-old flies (Fig. 1 and Dataset S2) and thus exhibited senescence. We also found significant genetic variation in phototaxis at each age, with broad sense heritabilities for the sexes pooled data of 0.27, 0.33, and 0.28 at 1, 2, and 4 wk, respectively (Fig. 1 and Dataset S2).

There is genetic variation in the magnitude and pattern of the decline in phototaxis behavior among the DGRP lines (that is, there is genetic variation in phototaxis senescence) because the line × age interaction term is significant in the ANOVA analyses (Dataset S2). Phenotypic (genetic) correlations (r) between phototaxis scores of 1- and 2-wk-old flies are 0.53 (0.64) and 0.61 (0.71) for females and males, respectively, but these correlations decline to 0.32 (0.39) and 0.35 (0.43) for females and males, respectively, when 1-wk-old and 4-wk-old flies are compared (Fig. 2 and Dataset S2). The departures of genetic correlations at different ages from unity (and equivalently, the significant line × age interaction terms for pairs of ages) indicate that the genetic architecture of phototaxis varies with age. Therefore, genetic variation in phototaxis senescence is partly (but not entirely) independent from that of genetic variation in phototaxis per se. Genetic variation in senescence could occur due to changes in variance in phototaxis and/or changes in rank order of phototaxis among the lines with age. We evaluated the relative magnitude of these two factors (47) and found that 97% of the genetic variance in senescence was due to changes of rank order among lines with age (Dataset S3). Therefore, the magnitude of senescence in phototaxis is not determined by the phototaxis response at a young age.

We observed significant sexual dimorphism in phototaxis. Averaged over all lines and ages, males have significantly higher phototaxis scores than females (Fig. 1 and Datasets S1 and S2). In addition, there is variation among the lines in the magnitude of this sexual dimorphism because the line × sex interaction term is significant in the analysis across three ages and for the analyses at weeks 2 and 4 (Dataset S2).

Phototaxis has both a visual and a locomotion component. To assess the extent to which we are assessing differences in vision among the lines as opposed to locomotion, we performed our phototaxis assay without a light source for 35 randomly selected DGRP lines at 1 wk of age (50 flies per sex). Under this condition, the flies showed little tendency to move out of the start tube, with average scores for both males and females <3.0 (Fig. S1 and Dataset S4). These scores are significantly lower than those obtained under similar conditions with a light stimulus ($P < 0.0001$, ANOVA) (Fig. S1 and Dataset S4), and the among-line and environmental variance are, respectively, 10-fold and eightfold smaller in the absence of a light cue (Dataset S4). Thus, directional responses measured in the countercurrent apparatus cannot be explained by differences in locomotion alone and therefore largely reflect vision-dependent behavior. Consistent

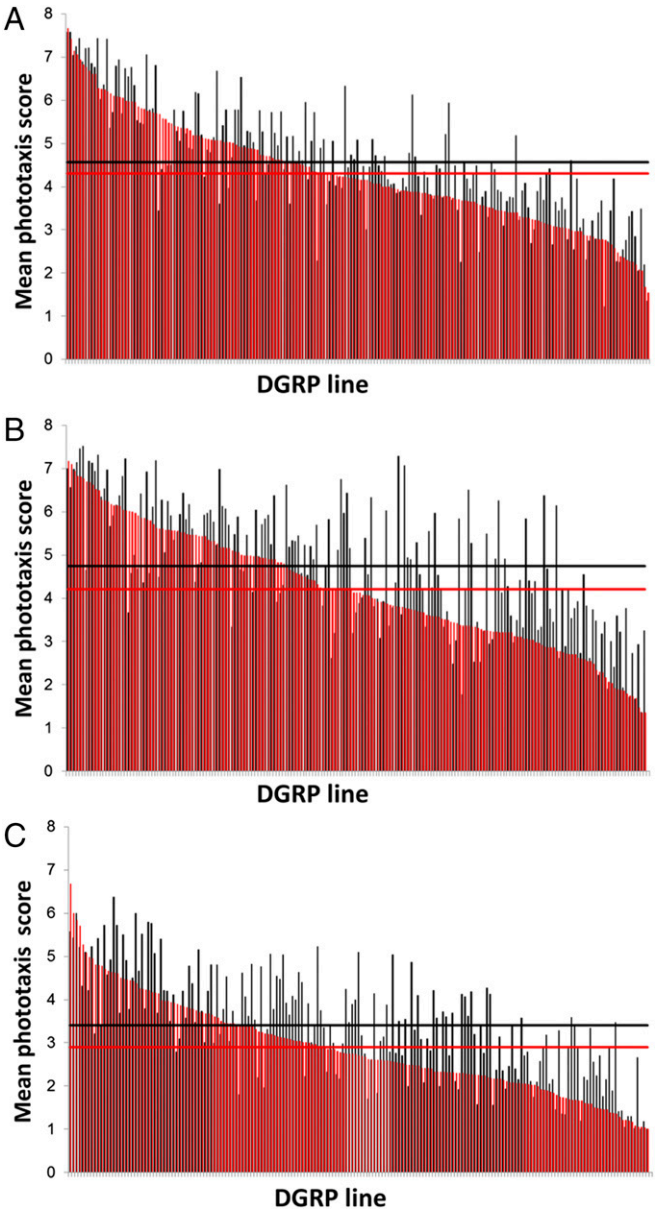

Fig. 1. Variation in phototaxis among the DGRP lines. Line means for phototaxis at (*A*) 1 wk, (*B*) 2 wk, and (*C*) 4 wk of age for females (red) and males (black). The plots are sorted by decreasing female score in each age group. The rank order differs between the ages. The horizontal red and black lines denote the average phototaxis score at each age for females and males, respectively: 1 wk: μ_F = 4.30, μ_M = 4.57; 2 wk: μ_F = 4.20, μ_M = 4.74; 4 wk: μ_F = 2.81, μ_M = 3.41.

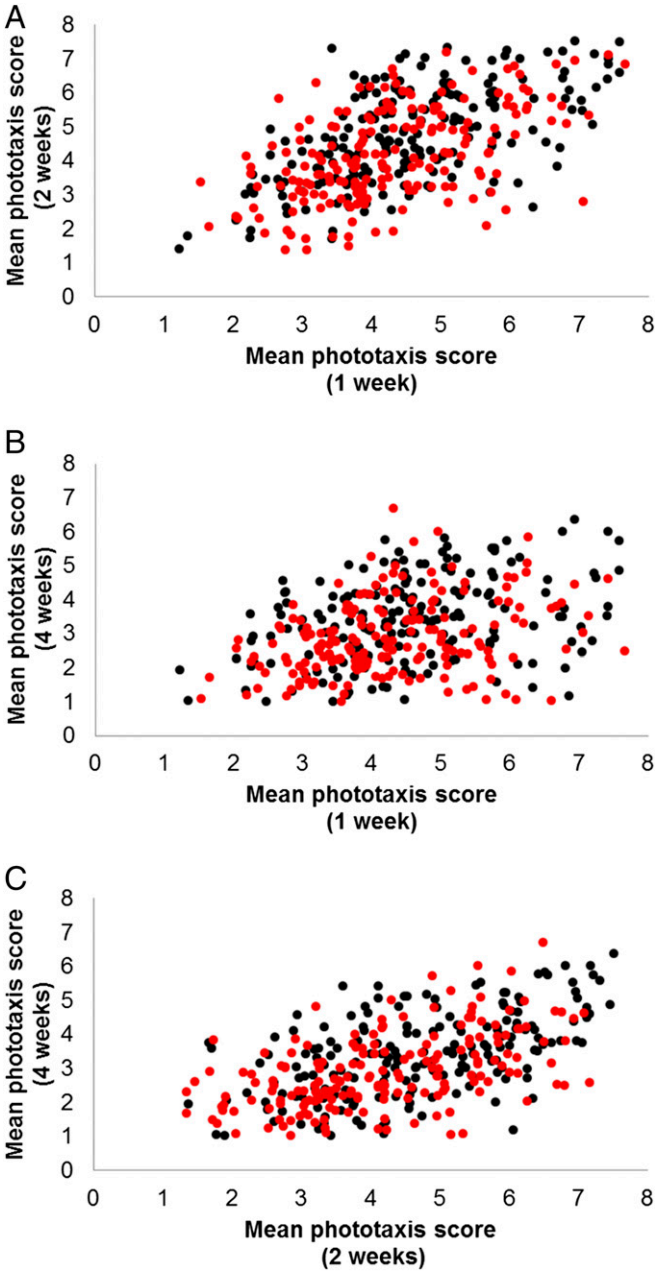

Fig. 2. Phenotypic correlation of phototaxis scores among the DGRP lines at different ages. Female and male scores are depicted in red and black, respectively. (*A*) Correlations between 1 and 2 wk are $r_P = 0.53$ (females) and $r_P = 0.61$ (males). (*B*) Correlations between 1 and 4 wk are $r_P = 0.32$ (females) and $r_P = 0.35$ (males). (*C*) Correlations between 2 and 4 wk are $r_P = 0.52$ (females) and $r_P = 0.61$ (males).

with these results, we observed a low yet significant phenotypic correlation between startle response, one measure of locomotor behavior (48), and phototaxis in the DGRP at 1 wk of age for females ($r = 0.27$, $P < 0.0001$) and males ($r = 0.35$, $P < 0.0001$). Therefore, only 7.4% of variation in phototaxis in females and 12.5% in males can be attributed to variation in locomotion in the DGRP.

GWA Mapping Analyses. We performed GWA analyses in the DGRP and in an AIP derived from 40 DGRP lines to identify candidate genes associated with variation for phototaxis and visual senescence. Because of the significant genetic variation in sexual dimorphism, we performed all GWA analyses for males and females separately. We performed separate GWA analyses for phototaxis at 1, 2, and 4 wk and for phototaxis values averaged over all three ages and averaged over weeks 1 and 2, 2 and 4, and 1 and 4. Genetic variation in age-dependent decline in phototaxis is indicated by the line × age interaction, which is equivalent to variation among lines in the mean difference in phototaxis between two ages. Therefore, we performed GWA analyses for visual senescence using the difference in phototaxis scores between weeks 1 and 2, 2 and 4, and 1 and 4. The DGRP GWA analyses evaluated single marker associations of line means with 1,876,781 common (minor allele frequency >0.05) variants after accounting for effects of *Wolbachia* infection, common polymorphic inversions, and polygenic relatedness (31). The GWA analyses in the AIP were based on an extreme quantitative trait locus (QTL) mapping design in which we evaluated differences in allele frequencies for 672,749–983,020 segregating variants (the numbers vary due to variation in sequence coverage and allele frequencies in the pools), from sequenced pools of flies with high and low phototaxis scores at 1, 2, and 4 wk of age (Fig. 3).

Using a strict Bonferroni correction for multiple tests ($P = 2.66 \times 10^{-8}$ for the DGRP GWA and $P = 6.25 \times 10^{-8}$ for the AIP GWA), we identified two closely linked intronic single nucleotide polymorphisms (SNPs) in *CG13004* associated with phototaxis in DGRP males. Using the same criterion, we identified eight SNPs associated with phototaxis in AIP females: two closely linked SNPs in a putative downstream regulatory region of *CG7294*; single intronic SNPs in *CG30158*, *CG42784*, *elk*, and *Msr-110*; a nonsynonymous coding polymorphism in *CG18622*; and one intergenic SNP (*3R*_11546727_SNP) (Dataset S5). We found 12 SNPs associated with phototaxis at a strict genome-wide significance level in AIP males: six intergenic SNPs (*2R*_20956774,

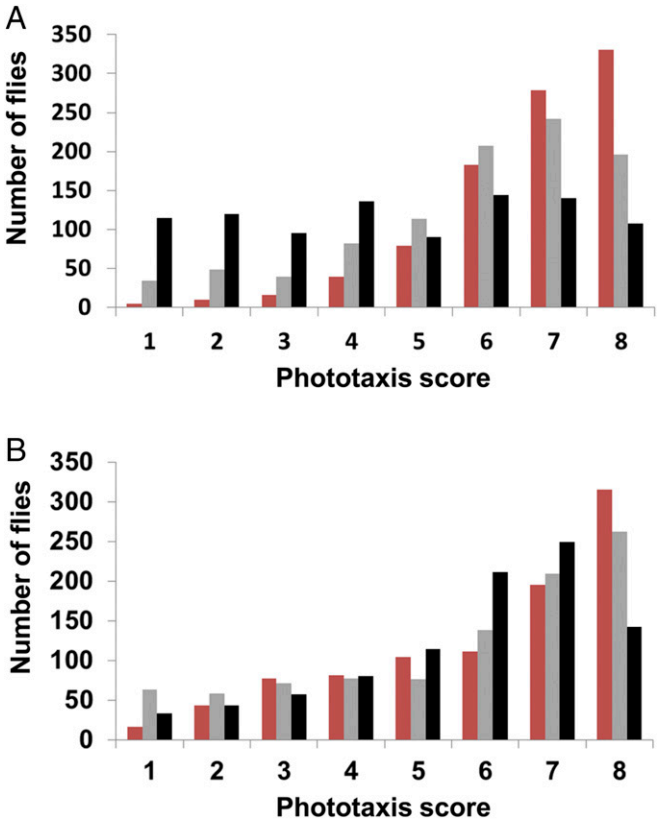

Fig. 3. Variation in phototaxis in the AIP. Frequency distributions of phototaxis scores are for a total of scores for 5,675 flies: ~950 individuals per age and sex. Red bars indicate 1-wk-old flies, gray bars indicate 2-wk-old flies, and black bars indicate 4-wk-old flies. (*A*) Females. (*B*) Males.

2R_8692474_SNP, 2R_8722202_SNP, 2R_9722208, 2R_8923692_SNP, and 3R_26087589_SNP); two closely linked intronic SNPs in *Drl-2*; and one intronic SNP in each of *cic*, *CG13830*, *CG14516*, and *Osi24* (Dataset S5). Only four SNPs were associated with phototaxis senescence at the Bonferroni-corrected significance level: the intergenic variant 2R_8722202_SNP and an intronic SNP in *Nos* for males and presumed regulatory SNPs in *Eno* and *CG13982* in females (Dataset S5). Thus, the majority of the most significant sequence variants appear to be associated with intergenic regions or in or near genes without functional annotations.

Notably, we observed minimal overlap in SNPs affecting phototaxis between ages. Only three SNPs were associated with variation in phototaxis at both 1 and 4 wk of age (Dataset S5): 2R_2797265_SNP, 2R_2797266_SNP, and 3R_8613417_SNP (intergenic). SNPs 2R_2797265 and 2R_2797266 are tightly linked and are located within an intron of *CG30158*. This gene is predicted to be involved in small GTPase mediated signal transduction (36). This lack of congruent SNPs among the ages indicates that different aspects of the genetic architecture contribute to variation in phototaxis with increasing age.

The advantage of the *Drosophila* system is that we can treat the GWA analyses as primary screens for candidate genes that can subsequently be validated by secondary analyses (29, 49). Using a more lenient reporting threshold of $P < 5 \times 10^{-5}$, we identified 3,319 unique variants, of which 2,553 map in or near 1,387 genes (the remaining variants are farther than 1 kb from the nearest gene) (Dataset S5). Gene ontology (GO) enrichment analysis of these candidate genes showed enrichment for transcription factors and for genes involved in learning and memory as well as development, especially development and function of the visual system and the nervous system in general (Dataset S6).

Genetic Interaction Networks. To prioritize candidate genes for subsequent functional analyses, we first asked whether they participated in known gene–gene interaction networks. Briefly, we mapped candidate genes onto known *Drosophila* genetic interaction networks and extracted subnetworks containing the candidate genes. We tested whether the size of the maximum subnetwork was significantly greater than expected by chance using a permutation procedure to obtain a *P* value for enrichment of the subnetwork for candidate

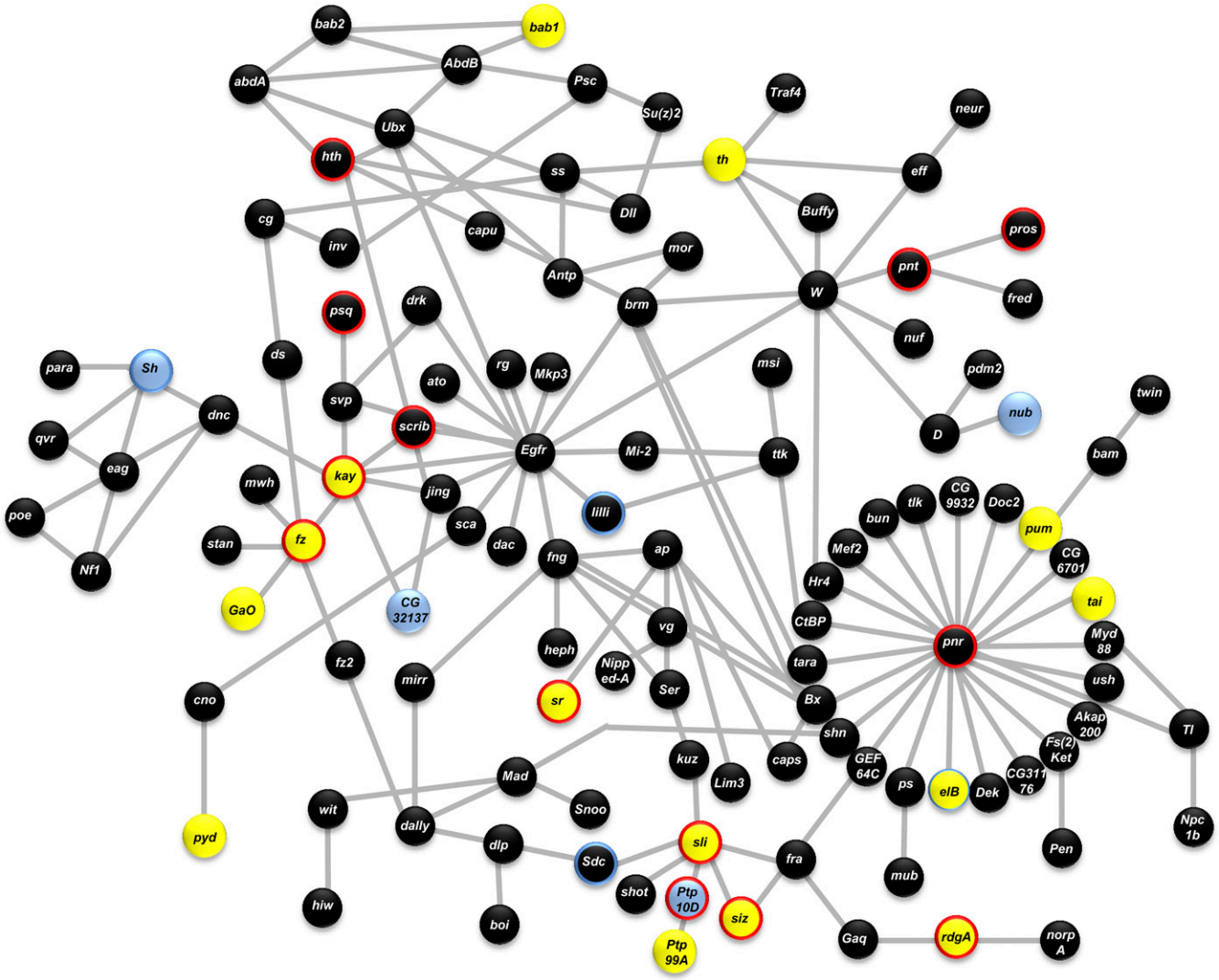

Fig. 4. Genetic interaction network of genes associated with phototaxis in the DGRP and AIP. Nodes depict genes, and edges are significant interactions. Black nodes depict genes identified in the AIP, blue nodes depict genes identified in the DGRP, and yellow nodes depict genes identified in both the DGRP and AIP mapping populations. The enrichment *P* value for the phototaxis network is 0.001. Nodes outlined in red were functionally validated using RNAi. Nodes outlined in light blue were tested using RNAi but did not have a significant effect on phototaxis.

genes. We performed three such analyses: one for candidate genes associated with variation in phototaxis, one for candidate genes associated with variation in senescent decline in phototaxis, and one for genes that appeared in two or more GWA analyses for either trait. Remarkably, all three analyses revealed gene interaction networks significantly enriched for GWA signals. The largest clusters of these gene interaction networks include 118 of the phototaxis candidate genes (Fig. 4; $P = 0.001$), 31 of the visual senescence candidate genes (Fig. 5; $P = 0.004$), and 56 candidate genes that appeared in two or more GWA analyses (Fig. S2; $P = 0.003$). Both the phototaxis and visual senescence networks were enriched for genes associated with early development, including eye and nervous system development (Fig. S3). Thus, genes associated with early development contribute to variation in both phototaxis and senescence for phototaxis behavior later in life.

Functional Validation Analyses. To assess whether mutations in genes that harbor SNPs associated with variation in phototaxis or age-dependent visual decline would affect these phenotypes, we selected 54 candidate genes as target genes for RNAi knockdown using an eye-specific driver and assessed to what extent suppression of gene expression affected phototaxis and/or phototaxis senescence. We chose these candidate genes based on their membership in one of the three enriched genetic interaction networks and/or gene ontology enrichment categories, P value in the GWA analyses, and availability of RNAi knockdown constructs. We measured phototaxis at 1, 2, and 4 wk of age for males and females and used factorial ANOVAs to assess whether they affected phototaxis (the line term) and/or phototaxis senescence (the line × age interaction term) relative to the control genotype. Remarkably, 49 of these candidate genes (90.7%) were nominally significant for phototaxis and/or phototaxis senescence in at least one of the three analyses (females, males, and pooled across sexes); and for 37 of these genes, the P values remained significant following a Bonferroni correction for multiple tests ($P < 9.26 \times 10^{-4}$) (Fig. 6 and Datasets S7 and S8). Most of the candidate genes showed reduced phototaxis at all ages relative to the control, indicating that normal expression of these genes is required for normal phototaxis. However, six candidate genes with significant effects on phototaxis senescence [*CG42671*, *king tubby* (*ktub*), *Patj*, *rau*, vein (*vn*), and *wntless* (*wls*)] had higher phototaxis scores than the control at 4 wk of age, suggesting that expression of these genes may promote visual decline. Human orthologs are known for 40 of the 49 significant candidate genes (Dataset S7). Seven of these genes are associated with eye diseases (Dataset S8).

Discussion

To characterize the genetic basis of naturally occurring variation for phototaxis and senescence for phototaxis behavior (as proxies for vision and visual decline, respectively), we performed quantitative genetic analyses in the inbred, sequenced DGRP lines as well as genome-wide association analyses in the DGRP and an AIP derived from the DGRP for these traits. We observe that as in humans, visual performance declines with age and thus exhibits senescence. There is significant naturally occurring genetic variation in phototaxis among the DGRP lines, as well as genetic variation among the DGRP lines in the extent to which they exhibit senescence for phototaxis. However, phototaxis senescence is only partially correlated with phototaxis averaged across all ages, such that phototaxis behavior early in life does not perfectly predict the magnitude of visual decline later in life. Genetic variation for mean life span among the DGRP lines has been reported previously (50), enabling us to evaluate the extent to which life span is associated with health span (in terms of variation for phototaxis senescence). The phenotypic correlation of life span with senescence in phototaxis between weeks 1 and 4 is low: 0.05 for females and 0.02 for males (Fig. S4). Thus, different physiological systems may undergo specific and independent senescence not correlated with organismal life span, and health span is not necessarily increased in long-lived genotypes.

We performed complementary GWA analyses in the DGRP and the outbred AIP, using complete sequence data. Only common variants with minor allele frequencies greater than 5% can be reliably interrogated in the DGRP, but the small size of the DGRP results in limited power to detect associations unless effects are very large. Sample size is not limiting in the AIP, and variants at

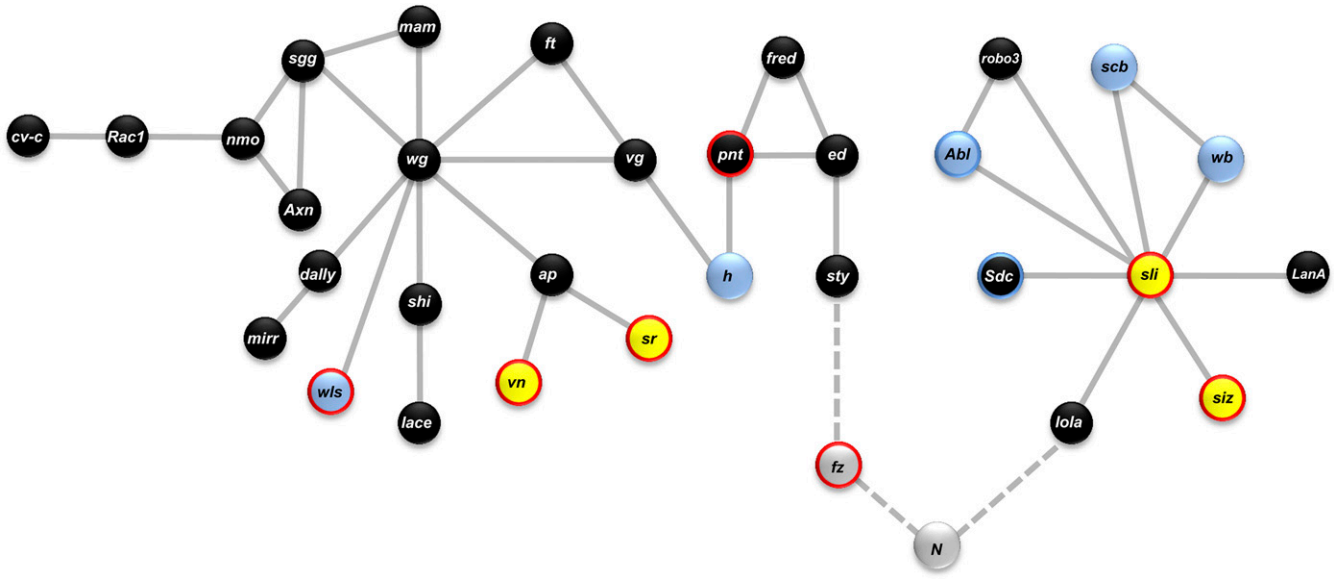

Fig. 5. Genetic interaction network of genes associated with phototaxis senescence in the DGRP and AIP. Nodes depict genes, and edges are significant interactions. Black nodes depict genes identified in the AIP, blue nodes depict genes identified in the DGRP, and yellow nodes depict genes identified in both the DGRP and AIP mapping populations. Gray nodes indicate missing genes and gray dashed lines depict their edges. The enrichment P value for the phototaxis senescence network is 0.004. Nodes outlined in red were functionally validated using RNAi. Nodes outlined in light blue were tested by using RNAi but did not have a significant effect on phototaxis senescence.

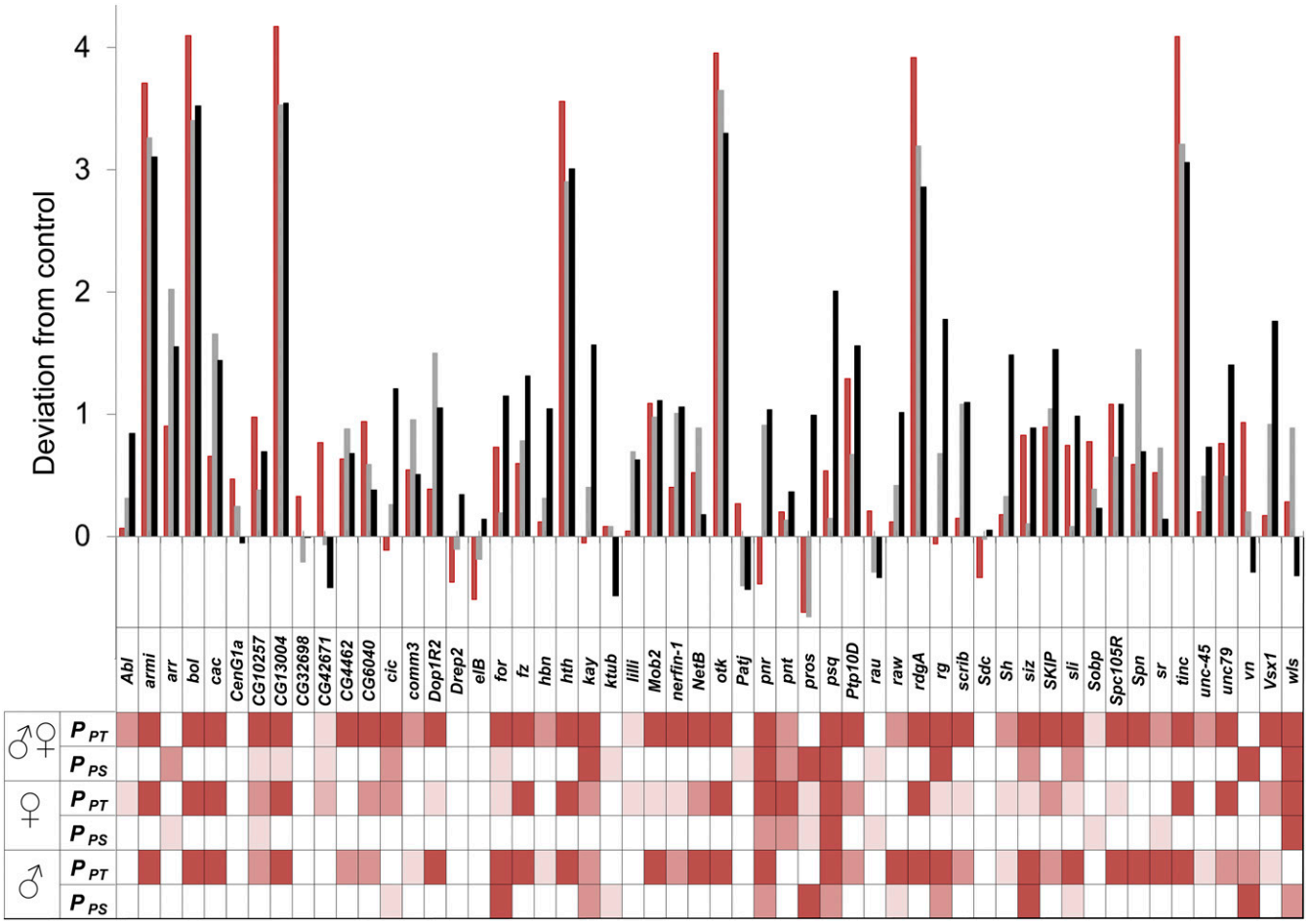

Fig. 6. Functional evaluation of candidate genes using RNAi suppression of gene expression. Histograms of sex-average phototaxis scores of F1 progeny from *gmr-Gal4* x *UAS*-RNAi for each of the genes indicated on the *x* axis. All phototaxis scores are expressed as deviations from the control. Red bars indicate 1 wk old, gray bars indicate 2 wk old, and black bars indicate 4 wk old. *P* values for phototaxis (P_{PT}) and phototaxis senescence (P_{PS}) are given for the analyses pooled across sexes (♂♀), females (♀), and males (♂). P_{PT} and P_{PS} correspond to the line and line × age *P* values, respectively, in Dataset S6. White indicates $P > 0.05$, light pink indicates $P < 0.05$, medium pink indicates $P < 0.01$, and dark pink indicates $P < 0.001$.

low frequency in the DGRP that are represented in at least one of the parental lines used to generate the AIP will have a minor allele frequency of at least 0.025 and hence can be evaluated if their frequencies in either the high or low pool are greater than 0.05. Although there are many reasons not to expect concordance between the two GWA analyses (24, 51), we do expect the top associations from both analyses will impinge on common genes and genetic networks. Indeed, 70 genes were in common between the two GWA analyses, suggesting a highly polygenic genetic architecture for phototaxis and phototaxis senescence.

A major advantage of the *Drosophila* model is that many genetic interactions have been documented experimentally (52). We therefore asked whether, and to what extent, the candidate genes identified by the GWA analyses were enriched for known genetic interactions. We performed these analyses for the candidate genes affecting phototaxis, senescence in phototaxis, and genes in common between the two GWA analyses for either trait. In each case we recovered enriched gene–gene interaction networks. These genetic interaction networks provide biological context for the many candidate genes identified by GWA analysis. Consistent with our observation from the quantitative genetic analysis indicating that phototaxis and senescence for phototaxis are only partly correlated, only 6 of the 31 genes in the phototaxis senescence network also appear in the phototaxis network.

Genes involved in insulin signaling and oxidative stress have been implicated as evolutionarily conserved mechanisms affecting life span in *Mus musculus* (53, 54), *Drosophila* (55–57), *Caenorhabditis elegans* (58, 59), and yeast (60, 61). Consistent with the lack of phenotypic correlation between phototaxis senescence and life span, we did not find genes associated with these mechanisms in our association analyses. Rather, candidate genes implicated by all GWA analyses as well as the subset of candidate genes in enriched genetic interaction networks were enriched for development and function of the visual and nervous systems. It should be noted that genes that contribute to development may have pleiotropic functions that play a role in adult life. Evidence from our study indicates that the same genes that affect early eye and nervous system development are associated with natural variation in visual decline at later age, highlighting the notion that senescence may be part of a lifelong developmental process.

We used RNAi-mediated knockdown of gene expression under the eye-specific *gmr-Gal4* driver to determine to what extent genes in the enriched genetic interaction networks that harbor polymorphisms associated with variation in phototaxis and visual senescence themselves affect these phenotypes. Disruption of expression of 49 of 54 tested target genes significantly affected phototaxis and/or phototaxis senescence. We are aware that RNAi is an imperfect proxy for testing effects of SNPs and that

the publicly available RNAi constructs cannot assess the effects of putative intronic and intergenic regulatory variants associated with phototaxis and phototaxis senescence, many of which had low *P* values in our association analyses. Although we do not expect the effects of RNAi to mimic the more subtle SNP effects in direction or magnitude, significance of these gene-level functional analyses can help to prioritize genes for future allelic replacement analyses using CRISPR/*Cas9* gene editing (62, 63) to determine causal SNPs.

The majority of the significant genes caused decreases in phototaxis at all ages relative to the control genotype, as expected if they are required for phototaxis. Several of these genes affect *Drosophila* eye development, although a role in adult phototaxis has not been reported previously. For example, the highly interconnected hub gene, *pnr*, which participates in 23 interactions in the phototaxis network (Fig. 4), encodes a GATA-1 transcription factor that regulates dorsal–ventral axis determination during *Drosophila* eye development and plays a role in defining the dorsal eye margin by downregulating the core retinal determination genes *eya*, *so*, and *dac* (64). *frizzled* (*fz*), *hth*, and *pros* function in the differentiation of cellular components of the compound eye such as ommatidia, photoreceptor, and rhabdomere cells, respectively, whereas *cacophony* (*cac*), *ktub*, *Mob2*, and *rdgA* play major roles in phototransduction (65–67). In addition, *cac* has previously been linked to life span in the DGRP (68) and to age-related decline in immune system function (69).

Several genes with significant effects on phototaxis senescence (*CG42671*, *ktub*, *Patj*, *rau*, *vn*, and *wls*) are particularly interesting because suppression of gene expression causes an increase in phototaxis at late ages, suggesting these genes normally function to exacerbate visual decline. *CG42671* is a computationally predicted gene about which nothing is known, so this study assigns a function. *vn* is a member of the epidermal growth factor receptor signaling pathway and functions in brain and PNS system development (70–72); it has not previously been implicated in phototaxis behavior. The other four genes have been associated with eye development and function. *ktub* mutations affect Rhodopsin 1 endocytosis and retinal degradation (73), *Patj* functions in photoreceptor cell morphogenesis and maintenance (74) and prevents late-onset photoreceptor degeneration, *rau* affects R7 photoreceptor cell development (75), and *wls* functions in Wnt protein binding and compound eye morphogenesis (76, 77).

The *Drosophila* compound eye is anatomically distinct from vertebrate eyes. To what extent do the genes in the genetic interaction networks identified in this study have human orthologs and are able to affect eye diseases in humans? A total of 41 of the validated candidate genes have human orthologs, 7 of which have previously been associated with vision disorders. *cac*, which encodes a calcium channel, has seven human orthologs that also encode calcium channel subunits, of which *CACNA1F* has been associated with congenital night blindness (*CSNB2A*) (78), Aland Island eye disease (*AIED*) (79, 80), and X-linked cone–rod dystrophy (*CORDX3*) (81). *fz* encodes a seven-transmembrane helix containing protein necessary for binding Wnt ligands in the noncanonical Wnt signaling pathway (82) and has 10 human orthologs encoding frizzled class receptors, of which *FZD4* is associated with exudative vitreoretinopathy (83). *hbn* encodes a transcription factor and has four human orthologs, of which *PHOX2A* has been associated with congenital fibrosis of extraocular muscles, a disorder that affects the muscles that control eye movement and position of the eyes (84, 85). *ktub* has three human orthologs, of which *TUB* is associated with retinal dystrophy and *TULP1* is associated with retinitis pigmentosa (86, 87) and Leber congenital amaurosis (early-onset retinal dystrophy) (88, 89). *NetB* encodes a protein with unknown molecular function and has nine human orthologs, of which *LAMC3* is associated with occipital cortical malformations, an autosomal recessive disorder with seizures associated with loss of vision due to the abnormal development of the occipital cortex (90). *unc-45* encodes a protein of unknown molecular function, but one of its human orthologs, *UNC45B*, has been associated with cataracts (91). *Vsx1* is a transcription factor with two human orthologs: *VSX1* is associated with keratoconus, anterior segment dysgenesis syndrome (which affect multiple eye tissues) (92, 93), and posterior polymorphous corneal dystrophy (94), whereas *VSX2* is associated with microphthalmia (95, 96). Thus, naturally occurring genetic variation affecting *Drosophila* phototaxis and senescence for phototaxis encompasses evolutionarily conserved genes that contribute to visual senescence in humans.

Materials and Methods

***Drosophila* Stocks and Culture.** We used 191 sequenced inbred DGRP lines (31, 46) and an AIP derived from 40 randomly selected DGRP lines. The 40 parental AIP lines were DGRP_21, DGRP_208, DGRP_301, DGRP_303, DGRP_304, DGRP_306, DGRP_307, DGRP_313, DGRP_315, DGRP_324, DGRP_335, DGRP_357, DGRP_358, DGRP_360, DGRP_362, DGRP_365, DGRP_375, DGRP_379, DGRP_380, DGRP_391, DGRP_399, DGRP_427, DGRP_437, DGRP_486, DGRP_517, DGRP_555, DGRP_639, DGRP_705, DGRP_707, DGRP_712, DGRP_714, DGRP_730, DGRP_732, DGRP_765, DGRP_774, DGRP_786, DGRP_799, DGRP_820, DGRP_852, and DGRP_859. At generation (G) 1, we crossed the AIP parent lines in a round robin design in numerical order; that is, we crossed DGRP_21 females to DGRP_208 males, DGRP_208 females to DGRP_301 males, and so on, finally crossing DGRP_859 females to DGRP_21 males. At G2, we performed another round robin cross using the heterozygous progeny from the first generation to create 40 four-DGRP parent genotypes; that is, we crossed G1 DGRP_21 × DGRP_208 females with G1 DGRP_301 × DGRP_303 males and so on until G1 DGRP_852 × DGRP_859 females were mated with G1 DGRP_21 × DGRP_208 males. At G3, we placed one male and one female of each genotype from the 40 four-DGRP parent genotypes into each of 10 bottles, removing the parents after 2 d. For each subsequent generation, we collected 4 males and 4 females from each of the 10 bottles from the previous generation and transferred them to 10 new bottles (40 males and 40 females total per new bottle). Therefore, the census size of the AIP population was $n = 800$ per generation. Experiments described here began at G120.

For functional assessment of candidate genes, we obtained *UAS*-RNAi lines from the KK or GD library stocks targeting candidate genes along with the progenitor coisogenic control line containing the empty vector (VIE-260B) from the Vienna *Drosophila* RNAi Center (VDRC) (37). We drove expression of RNAi in the fly eye using the *gmr-Gal4* driver line (genotype: w^{1118}; *P{GMR-GAL4.w-}2/CyO*) obtained from the Bloomington *Drosophila* Stock Center.

All flies were reared on cornmeal–agar–molasses medium at 25 °C, 60–75% relative humidity, and a 12-h light–dark cycle.

Phototaxis Measurements. We assessed phototaxis in the countercurrent apparatus designed by Benzer (40) at 1, 2, and 4 wk of age (representing young, middle-aged, and senior flies, respectively). For each of the genotypes (DGRP, AIP, or RNAi), we collected 50 age-matched flies of the same sex per replicate and performed three replicate assays. Flies were allowed to recover overnight from CO_2 anesthesia and dark-adapted for 30 min before performing the assay. To begin the assay, flies were tapped to the bottom of the first start tube, and the apparatus was laid horizontally with the distal tubes 5 cm from a 15-W fluorescent light. The flies were given 15 s to reach the distal tube. This procedure was repeated seven times, such that flies could choose to go toward the light a maximum of eight times. At the end of the trial, all eight start tubes containing flies were removed and frozen at −80 °C before manually counting the flies in each tube. Each individual fly is assigned a score from 1 (did not move toward the light) to 8 (moved toward the light seven times). Individual scores were used to conduct the quantitative genetic analyses described below. The mean phototaxis score for each replicate was calculated as $\sum(i \times Ni)/\sum Ni$, where Ni is the number of flies in the ith tube. To test locomotion in the dark, identical conditions were used but without a light source.

Quantitative Genetic Analyses. We partitioned the phenotypic variance of phototaxis in the DGRP into components attributable to genetic and environmental variance as well as genotype × sex, genotype × age, and the three-way genotype × age × line interactions using individual phototaxis data. The full mixed model analysis of variance (ANOVA) was $Y = \mu + L + S + A + L \times S + L \times A + S \times A + L \times S \times A + Rep(L \times S \times A) + \varepsilon$, where Y is the phenotype; μ is the overall mean; S and A are the fixed effects of sex and age, respectively; L is DGRP line (random); $L \times S$, $L \times A$, $S \times A$, and $L \times S \times A$ are the interaction terms; *Rep* is

replicate (random); and ε is the error variance. We estimated the broad-sense heritability (H^2) of phototaxis from the full model as $H^2 = (\sigma^2_L + \sigma^2_{L\times S} + \sigma^2_{L\times A} + \sigma^2_{L\times S\times A})/\sigma^2_L + \sigma^2_{L\times S} + \sigma^2_{L\times A} + \sigma^2_{L\times S\times A} + \sigma^2_\varepsilon$, where σ^2_L, $\sigma^2_{L\times S}$, $\sigma^2_{L\times A}$, $\sigma^2_{L\times S\times A}$, and σ^2_ε are the among-line, line × sex, line × age, line × sex × age, and within-line variance components, respectively.

We also ran reduced ANOVA models for sexes pooled across ages and for ages pooled across sexes. We estimated cross-age genetic correlations separately for males and females as $r_A = \sigma^2_L/(\sigma^2_L + \sigma^2_{L\times A})$ and cross-sex genetic correlations separately for each age as $r_S = \sigma^2_L/(\sigma^2_L + \sigma^2_{L\times S})$. We estimated the extent to which the $L \times A$ variance components are due to changes in variance in phototaxis among lines and changes in rank order as $\sigma^2_{L\times A} = \sum[2\sigma_{Li}\sigma_{Lj}(1 - r_{ij}) + (\sigma_{Li} - \sigma_{Lj})^2]/t(t-1)$, where $t = 3$ ages, σ_{Li} and σ_{Lj} are the square roots of the among-line variance components for ages i and j, and r_{ij} is the cross-age correlation among lines for ages i and j (47). The first term reflects the change in rank order among lines with age, whereas the second reflects differences in among-line variance with age.

GWA Analyses in the DGRP. We performed GWA analyses for phototaxis using (*i*) line means (average of replicate scores) at 1, 2, and 4 wk of age; (*ii*) the overall mean for all three ages; and (*iii*) means of 1 and 2 wk, 2 and 4 wk, and 1 and 4 wk. We also performed GWA analyses for senescence (*S*) in phototaxis using the mean differences in phototaxis scores between two different age groups: $S = (X_{ia} - X_{ib})/(\bar{X}_a + \bar{X}_b)/2$, where X is the mean phototaxis score of line i at the younger age (a) or corresponding older age (b) and $\bar{X}$ is the overall phototaxis mean among all DGRP lines at age a or b. GWA analyses for all traits were performed using a total of 1,876,781 variants, of which 1,716,060 were single-nucleotide and multinucleotide polymorphisms (SNPs/MNPs) and 160,721 were insertion–deletions (indels) for which the minor allele frequency is >0.05. Single-marker analyses were performed separately for males and females while accounting for any effects of *Wolbachia* infection, common polymorphic inversions, and polygenic relatedness, as described previously (31).

GWA Analyses in the AIP. Beginning at generation 120, we scored between 929 and 962 AIP flies per sex at 1, 2, and 4 wk of age and assayed these flies for phototaxis (5,675 flies in total). We pooled the top 100 (~10%) scoring flies (H) into one pool (sexes and ages separately) and the bottom 100 (~10%) scoring flies (L) into a second pool (sexes and ages separately). We sequenced DNA from each of the 12 pools to at least 50× coverage and assessed allele frequency differences between pools of individuals at the extremes of the distributions.

Genomic DNA was extracted from 100 pooled AIP flies per H and L sample, and high-molecular weight double-stranded genomic DNA samples were used to construct Illumina paired-end libraries. Briefly, 250 ng of DNA in a total volume of 8 μL was fragmented with NEBNext dsDNA Fragmentase (New England Biolabs) to an average size of 300–600 bp. Fragments were purified with 1.8× Agencourt AMPure XP beads (Beckman–Coulter) and then subjected to end-repair (Enzymatics), adenylation of 3′-ends (Enzymatics), and ligation of indexed paired-end adapters (Enzymatics and Bioo Scientific). Each step was followed by purification using 1.8× Agencourt AMPure XP beads (Beckman–Coulter). After ligation, size selection was carried out with 0.5× PEG/NaCl and purification with 0.1× Agencourt AMPure XP beads. PCR enrichment of the purified barcoded DNA was carried out with KAPA HiFi Hot Start Mix (Kapa Biosystems) and NEXTflex Primer Mix (Bioo Scientific). The libraries were quantified by quantitative PCR using the KAPA SYBR FAST Master Mix Universal 2× qPCR Master Mix (Kapa Biosystems). The sizes of the PCR-enriched libraries were quantified with an Agilent 2100 Bioanalyzer using the high-sensitivity DNA chip (Agilent). We multiplexed and sequenced four libraries per lane on the HiSeq2000 (Illumina) with v3 chemistry. Briefly, clonal clusters were generated on an Illumina C-Bot with Illumina's paired-end flow cell; 2 × 100 cycles of sequencing with 7 cycles index sequencing were carried out according to the manufacturer's standard protocol (Illumina). Imaging analysis and base calling were carried out with real time analysis (RTA) software on the HiSeq2000. Consensus assessment of sequence and variation (CASAVA) version 1.7 was used to demultiplex the sequences into fastq files that were used in the mapping analysis.

Sequence reads were mapped to the *D. melanogaster* reference genome (FlyBase version 5.57 of the Berkley Drosophila Genome Project assembly 5) using Burrows–Wheeler Alignment – maximal exact match (97) and subsequently indel-realigned, duplicate masked, and quality recalibrated using GATK (98). Alleles at segregating sites in the 40 parental lines were counted in the top (H) and bottom (L) pools, and their frequencies were compared ($f_H - f_L$) using a Z test (50). To obtain comparable tests to the GWA analyses in the DGRP that mapped variants for average phototaxis across ages or senescence, the average $f_H - f_L$ or differences in $f_H - f_L$ across ages were also tested using a Z test.

Mapping Genes to Networks. We downloaded the complete genetic interaction networks from FlyBase (Release 5.49) which were curated based on the literature. The genes in the networks are represented as nodes, whereas edges between the nodes represent interactions. We performed three separate analyses mapping candidate genes implicated by the GWA analyses for (*i*) phototaxis, (*ii*) phototaxis senescence, and (*iii*) all candidate genes that were implicated at least twice in the GWA analyses to the graphical representation of genetic networks using the igraph package in R (99). By allowing 0 missing nodes, subnetworks involving the candidate genes were extracted. We tested whether the maximum subnetwork was significantly greater than expected by chance using a permutation procedure (100). Briefly, we randomly selected n genes that can be mapped to the global networks, where n is the number of significant genes mapped to the global network. The size of the largest subnetwork was computed. This procedure was repeated 1,000 times, and the P value was calculated as $(A + 1)/1{,}001$, where A was the number of permutations where the size of the largest subnetwork was equal or greater than the size of the largest subnetwork with the observed gene list.

To identify biological processes associated with phototaxis and visual senescence, we performed enrichment analyses for gene ontologies using candidate gene lists from both the GWAS and extreme QTL mapping for both traits, using the Database for Annotation, Visualization and Integrated Discovery (101, 102). We also performed enrichment analyses on genes in the interaction networks.

Candidate Gene Validation. We selected candidate genes for phenotypic validation based on three criteria: (*i*) the candidate gene was identified in two or more DGRP and/or AIP GWA analyses ($P < 5 \times 10^{-5}$), (*ii*) candidate genes belonged to a significant genetic interaction network, and (*iii*) viable RNAi knockdown lines were available from the VDRC (37). Males from each of the transgenic *UAS*-RNAi lines were crossed to virgin females from the *gmr-Gal4* driver line to suppress the expression of the target gene in hybrid offspring. We assessed phototaxis in *gmr-Gal4/UAS-RNAi* and *gmr-Gal4/*VIE-260B control genotypes at 1, 2, and 4 wk of age. We assessed statistically significant differences in phototaxis between the RNAi knockdown and control genotypes using the mixed model ANOVA: $Y = \mu + G + S + A + G\times S + G\times A + S\times A + G\times S\times A + Rep(G\times S\times A) + \varepsilon$, where Y is the phenotype; μ is the overall mean; S and A are the fixed effects of sex and age, respectively; G is RNAi knockdown or control genotype (fixed); $G\times S$, $G\times A$, $S\times A$, and $G\times S\times A$ are the interaction terms (fixed); *Rep* is replicate (random); and ε is the error variance.

ACKNOWLEDGMENTS. This work was funded by National Institutes of Health Grant R01 AG043490 (to T.F.C.M. and R.R.H.A.).

1. Ding X, Patel M, Chan CC (2009) Molecular pathology of age-related macular degeneration. *Prog Retin Eye Res* 28(1):1–18.
2. West S (2007) Epidemiology of cataract: Accomplishments over 25 years and future directions. *Ophthalmic Epidemiol* 14(4):173–178.
3. Paulus YM, Gariano RF (2009) Diabetic retinopathy: A growing concern in an aging population. *Geriatrics* 64(2):16–20.
4. Coleman AL, Miglior S (2008) Risk factors for glaucoma onset and progression. *Surv Ophthalmol* 53(Suppl1):S3–S10.
5. Rosenberg EA, Sperazza LC (2008) The visually impaired patient. *Am Fam Physician* 77(10):1431–1436.
6. Carbone MA, et al. (2009) Overexpression of myocilin in the *Drosophila* eye activates the unfolded protein response: Implications for glaucoma. *PLoS One* 4(1):e4216.
7. Ryoo HD, Domingos PM, Kang MJ, Steller H (2007) Unfolded protein response in a *Drosophila* model for retinal degeneration. *EMBO J* 26(1):242–252.
8. Shen X, Ying H, Yue BY (2012) Wnt activation by wild type and mutant myocilin in cultured human trabecular meshwork cells. *PLoS One* 7(9):e44902.
9. Kwon HS, Lee HS, Ji Y, Rubin JS, Tomarev SI (2009) Myocilin is a modulator of Wnt signaling. *Mol Cell Biol* 29(8):2139–2154.
10. Kang KH, Lemke G, Kim JW (2009) The PI3K-PTEN tug-of-war, oxidative stress and retinal degeneration. *Trends Mol Med* 15(5):191–198.
11. He Y, et al. (2008) Mitochondrial complex I defect induces ROS release and degeneration in trabecular meshwork cells of POAG patients: Protection by antioxidants. *Invest Ophthalmol Vis Sci* 49(4):1447–1458.
12. Kong GY, Van Bergen NJ, Trounce IA, Crowston JG (2009) Mitochondrial dysfunction and glaucoma. *J Glaucoma* 18(2):93–100.
13. Datta R, Waheed A, Bonapace G, Shah GN, Sly WS (2009) Pathogenesis of retinitis pigmentosa associated with apoptosis-inducing mutations in carbonic anhydrase IV. *Proc Natl Acad Sci USA* 106(9):3437–3442.

14. Waller EA, Bendel RE, Kaplan J (2008) Sleep disorders and the eye. *Mayo Clin Proc* 83(11):1251–1261.
15. Mackay TFC, Anholt RRH (2006) Of flies and man: *Drosophila* as a model for human complex traits. *Annu Rev Genomics Hum Genet* 7:339–367.
16. Iijima K, Iijima-Ando K (2008) *Drosophila* models of Alzheimer's amyloidosis: The challenge of dissecting the complex mechanisms of toxicity of amyloid-beta 42. *J Alzheimers Dis* 15(4):523–540.
17. Feany MB, Bender WW (2000) A *Drosophila* model of Parkinson's disease. *Nature* 404(6776):394–398.
18. Lee WC, Yoshihara M, Littleton JT (2004) Cytoplasmic aggregates trap polyglutamine-containing proteins and block axonal transport in a *Drosophila* model of Huntington's disease. *Proc Natl Acad Sci USA* 101(9):3224–3229.
19. De Luca M, et al. (2003) *Dopa decarboxylase* (*Ddc*) affects variation in *Drosophila* longevity. *Nat Genet* 34(4):429–433.
20. Harbison ST, et al. (2009) Co-regulated transcriptional networks contribute to natural genetic variation in *Drosophila* sleep. *Nat Genet* 41(3):371–375.
21. Chen S, Lee AY, Bowens NM, Huber R, Kravitz EA (2002) Fighting fruit flies: A model system for the study of aggression. *Proc Natl Acad Sci USA* 99(8):5664–5668.
22. Edwards AC, Mackay TFC (2009) Quantitative trait loci for aggressive behavior in *Drosophila melanogaster*. *Genetics* 182(3):889–897.
23. Kravitz EA, Fernandez MdeL (2015) Aggression in *Drosophila*. *Behav Neurosci* 129(5): 549–563.
24. Shorter J, et al. (2015) Genetic architecture of natural variation in *Drosophila melanogaster* aggressive behavior. *Proc Natl Acad Sci USA* 112(27):E3555–E3563.
25. Ghezzi A, et al. (2013) Alcohol-induced histone acetylation reveals a gene network involved in alcohol tolerance. *PLoS Genet* 9(12):e1003986.
26. Liao J, Seggio JA, Ahmad ST (2016) Mutations in the circadian gene period alter behavioral and biochemical responses to ethanol in *Drosophila*. *Behav Brain Res* 302: 213–219.
27. Morozova TV, Anholt RRH, Mackay TFC (2007) Phenotypic and transcriptional response to selection for alcohol sensitivity in *Drosophila melanogaster*. *Genome Biol* 8(10):R231.
28. Morozova TV, et al. (2009) Alcohol sensitivity in *Drosophila*: Translational potential of systems genetics. *Genetics* 183(2):733–745, 1SI–12SI.
29. Morozova TV, et al. (2015) Polymorphisms in early neurodevelopmental genes affect natural variation in alcohol sensitivity in adult *drosophila*. *BMC Genomics* 16(1):865.
30. Morozova TV, Mackay TFC, Anholt RRH (2011) Transcriptional networks for alcohol sensitivity in *Drosophila melanogaster*. *Genetics* 187(4):1193–1205.
31. Huang W, et al. (2014) Natural variation in genome architecture among 205 *Drosophila melanogaster* Genetic Reference Panel lines. *Genome Res* 24(7):1193–1208.
32. Swarup S, Huang W, Mackay TFC, Anholt RRH (2013) Analysis of natural variation reveals neurogenetic networks for *Drosophila* olfactory behavior. *Proc Natl Acad Sci USA* 110(3):1017–1022.
33. Weber AL, et al. (2012) Genome-wide association analysis of oxidative stress resistance in *Drosophila melanogaster*. *PLoS One* 7(4):e34745.
34. Zwarts L, et al. (2011) Complex genetic architecture of *Drosophila* aggressive behavior. *Proc Natl Acad Sci USA* 108(41):17070–17075.
35. Adams MD, et al. (2000) The genome sequence of *Drosophila melanogaster*. *Science* 287(5461):2185–2195.
36. Drysdale RA, Crosby MA; FlyBase Consortium (2005) FlyBase: Genes and gene models. *Nucleic Acids Res* 33(Database issue):D390–D395.
37. Dietzl G, et al. (2007) A genome-wide transgenic RNAi library for conditional gene inactivation in *Drosophila*. *Nature* 448(7150):151–156.
38. Parks AL, et al. (2004) Systematic generation of high-resolution deletion coverage of the *Drosophila melanogaster* genome. *Nat Genet* 36(3):288–292.
39. Thibault ST, et al. (2004) A complementary transposon tool kit for *Drosophila melanogaster* using *P* and *piggyBac*. *Nat Genet* 36(3):283–287.
40. Benzer S (1967) Behavioral mutants of *Drosophila* isolated by countercurrent distribution. *Proc Natl Acad Sci USA* 58(3):1112–1119.
41. Markow TA, Merriam J (1977) Phototactic and geotactic behavior of countercurrent defective mutants of *Drosophila melanogaster*. *Behav Genet* 7(6):447–455.
42. Zhu Y (2013) The *Drosophila* visual system: From neural circuits to behavior. *Cell Adhes Migr* 7(4):333–344.
43. Grotewiel MS, Martin I, Bhandari P, Cook-Wiens E (2005) Functional senescence in *Drosophila melanogaster*. *Ageing Res Rev* 4(3):372–397.
44. Luan Z, Reddig K, Li HS (2014) Loss of Na(+)/K(+)-ATPase in *Drosophila* photoreceptors leads to blindness and age-dependent neurodegeneration. *Exp Neurol* 261: 791–801.
45. Simon AF, Liang DT, Krantz DE (2006) Differential decline in behavioral performance of *Drosophila melanogaster* with age. *Mech Ageing Dev* 127(7):647–651.
46. Mackay TFC, et al. (2012) The *Drosophila melanogaster* Genetic Reference Panel. *Nature* 482(7384):173–178.
47. Cockerham CC (1963) Estimation of genetic variances. *Statistical Genetics and Plant Breeding*, eds Hanson WD, Robinson HF (National Academy of Sciences–National Research Council, Washington, DC), pp 53–94.
48. Jordan KW, Carbone MA, Yamamoto A, Morgan TJ, Mackay TF (2007) Quantitative genomics of locomotor behavior in *Drosophila melanogaster*. *Genome Biol* 8(8): R172.
49. Arya GH, et al. (2015) The genetic basis for variation in olfactory behavior in *Drosophila melanogaster*. *Chem Senses* 40(4):233–243.
50. Ivanov DK, et al. (2015) Longevity GWAS using the *Drosophila* Genetic Reference Panel. *J Gerontol A Biol Sci Med Sci* 70(12):1470–1478.
51. Huang W, et al. (2012) Epistasis dominates the genetic architecture of *Drosophila* quantitative traits. *Proc Natl Acad Sci USA* 109(39):15553–15559.
52. Attrill H, et al.; FlyBase Consortium (2016) FlyBase: Establishing a Gene Group resource for *Drosophila melanogaster*. *Nucleic Acids Res* 44(D1):D786–D792.
53. Wiesenborn DS, Ayala JE, King E, Masternak MM (2014) Insulin sensitivity in long-living Ames dwarf mice. *Age (Dordr)* 36(5):9709.
54. Selman C, et al. (2008) Evidence for lifespan extension and delayed age-related biomarkers in insulin receptor substrate 1 null mice. *FASEB J* 22(3):807–818.
55. Clancy DJ, et al. (2001) Extension of life-span by loss of CHICO, a *Drosophila* insulin receptor substrate protein. *Science* 292(5514):104–106.
56. Giannakou ME, et al. (2004) Long-lived *Drosophila* with overexpressed dFOXO in adult fat body. *Science* 305(5682):361.
57. Hwangbo DS, Gershman B, Tu MP, Palmer M, Tatar M (2004) *Drosophila* dFOXO controls lifespan and regulates insulin signalling in brain and fat body. *Nature* 429(6991):562–566.
58. Bansal A, et al. (2014) Transcriptional regulation of *Caenorhabditis elegans* FOXO/DAF-16 modulates lifespan. *Longev Healthspan* 3:5.
59. Tullet JM, et al. (2014) DAF-16/FoxO directly regulates an atypical AMP-activated protein kinase gamma isoform to mediate the effects of insulin/IGF-1 signaling on aging in *Caenorhabditis elegans*. *PLoS Genet* 10(2):e1004109.
60. Kaeberlein M, McVey M, Guarente L (1999) The SIR2/3/4 complex and SIR2 alone promote longevity in *Saccharomyces cerevisiae* by two different mechanisms. *Genes Dev* 13(19):2570–2580.
61. Lin SJ, Defossez PA, Guarente L (2000) Requirement of NAD and SIR2 for life-span extension by calorie restriction in *Saccharomyces cerevisiae*. *Science* 289(5487): 2126–2128.
62. Zhang X, Koolhaas WH, Schnorrer F (2014) A versatile two-step CRISPR- and RMCE-based strategy for efficient genome engineering in *Drosophila*. *G3 (Bethesda)* 4(12): 2409–2418.
63. Yu Z, et al. (2013) Highly efficient genome modifications mediated by CRISPR/Cas9 in *Drosophila*. *Genetics* 195(1):289–291.
64. Oros SM, Tare M, Kango-Singh M, Singh A (2010) Dorsal eye selector *pannier* (*pnr*) suppresses the eye fate to define dorsal margin of the *Drosophila* eye. *Dev Biol* 346(2):258–271.
65. Masai I, Suzuki E, Yoon CS, Kohyama A, Hotta Y (1997) Immunolocalization of *Drosophila* eye-specific diacylgylcerol kinase, *rdgA*, which is essential for the maintenance of the photoreceptor. *J Neurobiol* 32(7):695–706.
66. Montell C (2005) TRP channels in *Drosophila* photoreceptor cells. *J Physiol* 567(Pt 1): 45–51.
67. Chorna-Ornan I, et al. (2005) Light-regulated interaction of Dmoesin with TRP and TRPL channels is required for maintenance of photoreceptors. *J Cell Biol* 171(1): 143–152.
68. Durham MF, Magwire MM, Stone EA, Leips J (2014) Genome-wide analysis in *Drosophila* reveals age-specific effects of SNPs on fitness traits. *Nat Commun* 5:4338.
69. Felix TM, Hughes KA, Stone EA, Drnevich JM, Leips J (2012) Age-specific variation in immune response in *Drosophila melanogaster* has a genetic basis. *Genetics* 191(3): 989–1002.
70. Schnepp B, Grumbling G, Donaldson T, Simcox A (1996) Vein is a novel component in the *Drosophila* epidermal growth factor receptor pathway with similarity to the neuregulins. *Genes Dev* 10(18):2302–2313.
71. Sepp KJ, Auld VJ (2003) Reciprocal interactions between neurons and glia are required for *Drosophila* peripheral nervous system development. *J Neurosci* 23(23): 8221–8230.
72. Page DT (2003) A function for Egf receptor signaling in expanding the developing brain in *Drosophila*. *Curr Biol* 13(6):474–482.
73. Chen SF, Tsai YC, Fan SS (2012) *Drosophila king tubby* (*ktub*) mediates light-induced rhodopsin endocytosis and retinal degeneration. *J Biomed Sci* 19:101.
74. Nam SC, Choi KW (2006) Domain-specific early and late function of Dpatj in *Drosophila* photoreceptor cells. *Dev Dyn* 235(6):1501–1507.
75. Sieglitz F, et al. (2013) Antagonistic feedback loops involving Rau and Sprouty in the *Drosophila* eye control neuronal and glial differentiation. *Sci Signal* 6(300):ra96.
76. Goodman RM, et al. (2006) Sprinter: A novel transmembrane protein required for Wg secretion and signaling. *Development* 133(24):4901–4911.
77. Bartscherer K, Pelte N, Ingelfinger D, Boutros M (2006) Secretion of Wnt ligands requires Evi, a conserved transmembrane protein. *Cell* 125(3):523–533.
78. Boycott KM, et al. (2001) A summary of 20 CACNA1F mutations identified in 36 families with incomplete X-linked congenital stationary night blindness, and characterization of splice variants. *Hum Genet* 108(2):91–97.
79. Alitalo T, Kruse TA, Forsius H, Eriksson AW, de la Chapelle A (1991) Localization of the Aland Island eye disease locus to the pericentromeric region of the X chromosome by linkage analysis. *Am J Hum Genet* 48(1):31–38.
80. Glass IA, et al. (1993) Genetic mapping of a cone and rod dysfunction (Aland Island eye disease) to the proximal short arm of the human X chromosome. *J Med Genet* 30(12):1044–1050.
81. Jalkanen R, et al. (2006) X linked cone-rod dystrophy, *CORDX3*, is caused by a mutation in the *CACNA1F* gene. *J Med Genet* 43(8):699–704.
82. Dijksterhuis JP, Petersen J, Schulte G (2014) WNT/Frizzled signalling: Receptor-ligand selectivity with focus on FZD-G protein signalling and its physiological relevance: IUPHAR Review 3. *Br J Pharmacol* 171(5):1195–1209.
83. Milhem RM, Ben-Salem S, Al-Gazali L, Ali BR (2014) Identification of the cellular mechanisms that modulate trafficking of *frizzled family receptor 4* (*FZD4*) missense mutants associated with familial exudative vitreoretinopathy. *Invest Ophthalmol Vis Sci* 55(6):3423–3431.
84. Wang SM, et al. (1998) Congenital fibrosis of the extraocular muscles type 2, an inherited exotropic strabismus fixus, maps to distal 11q13. *Am J Hum Genet* 63(2): 517–525.

85. Nakano M, et al. (2001) Homozygous mutations in *ARIX*(*PHOX2A*) result in congenital fibrosis of the extraocular muscles type 2. *Nat Genet* 29(3):315–320.
86. Banerjee P, et al. (1998) TULP1 mutation in two extended Dominican kindreds with autosomal recessive retinitis pigmentosa. *Nat Genet* 18(2):177–179.
87. den Hollander AI, et al. (2007) Novel compound heterozygous *TULP1* mutations in a family with severe early-onset retinitis pigmentosa. *Arch Ophthalmol* 125(7): 932–935.
88. den Hollander AI, et al. (2007) Identification of novel mutations in patients with Leber congenital amaurosis and juvenile RP by genome-wide homozygosity mapping with SNP microarrays. *Invest Ophthalmol Vis Sci* 48(12):5690–5698.
89. Mataftsi A, et al. (2007) Novel *TULP1* mutation causing leber congenital amaurosis or early onset retinal degeneration. *Invest Ophthalmol Vis Sci* 48(11):5160–5167.
90. Barak T, et al. (2011) Recessive LAMC3 mutations cause malformations of occipital cortical development. *Nat Genet* 43(6):590–594.
91. Hansen L, et al. (2014) The myosin chaperone *UNC45B* is involved in lens development and autosomal dominant juvenile cataract. *Eur J Hum Genet* 22(11):1290–1297.
92. Bisceglia L, et al. (2005) VSX1 mutational analysis in a series of Italian patients affected by keratoconus: Detection of a novel mutation. *Invest Ophthalmol Vis Sci* 46(1):39–45.
93. Dash DP, et al. (2010) Mutational screening of *VSX1* in keratoconus patients from the European population. *Eye (Lond)* 24(6):1085–1092.
94. Héon E, et al. (2002) *VSX1*: A gene for posterior polymorphous dystrophy and keratoconus. *Hum Mol Genet* 11(9):1029–1036.
95. Bar-Yosef U, et al. (2004) *CHX10* mutations cause non-syndromic microphthalmia/anophthalmia in Arab and Jewish kindreds. *Hum Genet* 115(4):302–309.
96. Faiyaz-Ul-Haque M, et al. (2007) Mutations in the *CHX10* gene in non-syndromic microphthalmia/anophthalmia patients from Qatar. *Clin Genet* 72(2):164–166.
97. Li H, Durbin R (2010) Fast and accurate long-read alignment with Burrows-Wheeler transform. *Bioinformatics* 26(5):589–595.
98. DePristo MA, et al. (2011) A framework for variation discovery and genotyping using next-generation DNA sequencing data. *Nat Genet* 43(5):491–498.
99. R Core Team (2016) *R: A Language and Environment for Statistical Computing* (R Foundation for Statistical Computing, Vienna).
100. Antonov AV, Dietmann S, Mewes HW (2008) KEGG spider: Interpretation of genomics data in the context of the global gene metabolic network. *Genome Biol* 9(12): R179.
101. Huang W, Sherman BT, Lempicki RA (2009) Systematic and integrative analysis of large gene lists using DAVID bioinformatics resources. *Nat Protoc* 4(1):44–57.
102. Huang W, Sherman BT, Lempicki RA (2009) Bioinformatics enrichment tools: Paths toward the comprehensive functional analysis of large gene lists. *Nucleic Acids Res* 37(1):1–13.